Scanning-tunneling-microscopy investigation of the $p(2\times2)$ and $c(2\times2)$ overlayers of S on Ni(100)

A. Partridge,* G. J. Tatlock, F. M. Leibsle, and C. F. J. Flipse*
IRC for Surface Science, University of Liverpool, P.O. Box 147, Liverpool L69 3BX, United Kingdom

G. Hörmandinger and J. B. Pendry
Department of Physics, Blackett Laboratories, Imperial College, London SW7 2BZ, United Kingdom
(Received 21 September 1992; revised manuscript received 26 January 1993)

The $p(2\times2)$ and $c(2\times2)$ sulfur overlayers on Ni(100), and the clean Ni(100) surface itself, have been imaged in an ultrahigh-vacuum scanning tunneling microscope and topographic and spectroscopic information was obtained from all three surfaces. These data are compared to theoretical calculations of the surfaces derived using the Green's-function method of Pendry, Pretre, and Krutzen, where the sample Green's function is calculated in a multiple-scattering formalism based on the layer Korringa-Kohn-Rostoker method. Our simple model has proved reasonably successful in predicting the corrugation heights observed on the sulfated nickel surfaces, and confirmed the fact that the difference in height observed between the $p(2\times2)$ and the $c(2\times2)$ phases is electronic in origin. It is also proposed that the enhanced corrugation observed on the clean nickel surface may in part be attributable to the presence of a magnetic surface state immediately below the Fermi energy. Attempts to model the I-V and dI/dV spectroscopy curves proved less successful but it is believed that this was largely attributable to the approximations used in the present calculation.

I. INTRODUCTION

The adsorption of gases onto the low index surfaces of metals has been extensively studied over recent years. The motivation to study these systems has been provided by a fundamental interest in adsorbate-substrate reactions. However, the Ni-S system is of particular interest due to the well-known poisoning effect of sulfur on certain catalytic reactions occurring on the clean nickel surface.[1,2] As a result of the interest generated in the nickel-sulfur system, and as a consequence of its widespread use as a model adsorption system, extensive investigations of both the geometric and electronic structure of the $p(2\times2)$S and $c(2\times2)$S surfaces have been carried out. The adsorption site of the sulfur atoms and the subsequent substrate relaxation has been studied by a variety of experimental techniques (low-energy electron diffraction,[3] surface and near-edge x-ray-adsorption fine structure,[4–7] photoelectron diffraction,[8] impact collision ion-scattering spectroscopy,[9] and angle-resolved photoelectron fine structure[10]), while the changes in the electronic structure of the surface following adsorption have been investigated by both experimental (ultraviolet photoelectron spectroscopy,[11–13] inverse photoemission,[14] ion neutralization spectroscopy[15]) and theoretical techniques.[16]

The development of the scanning tunneling microscope (STM) over the last few years has provided an additional method of investigating the surfaces of a variety of materials. Initially, these STM investigations concentrated primarily on semiconductor materials, but more recently both metal and metal-gas adsorption systems have been extensively studied.[17] These investigations have stimulated interest in the theoretical calculation of STM images on both clean and adsorbate-covered metal surfaces, including the sulfur-nickel system. Although some studies of sulfur-metal systems have been carried out,[18–20] to our knowledge no investigation of the sulfur-nickel system has been performed. Therefore this study was carried out to provide further information on the S-Ni surface and to provide empirical data which have been used as a benchmark for theoretical calculations of the STM images and spectra on both the clean and sulfated nickel surfaces. The STM images and spectroscopy curves produced were simulated using a description of the STM based on the theory of Pendry, Pretre, and Krutzen,[21] where the sample Green's function is calculated in a multiple-scattering formalism based on the layer Korringa-Kohn-Rostoker (KKR) method.[22] An analysis and discussion of the experimental results and theoretical calculations is presented in the following sections.

The paper has been broken down into four main sections. Section II briefly reviews the experimental techniques used. Section III discusses the experimental results obtained with the STM, using both topographic and spectroscopic analysis modes on the clean and sulfated surfaces. Section IV outlines the theory used to interpret the STM images and spectra, while Sec. V discusses the results obtained using these calculations and compares them with the experimental results.

II. EXPERIMENTAL TECHNIQUES

A high-purity nickel single crystal was obtained which had been sectioned such that the surface plane had a [100] surface normal. The crystal was prepared by flashing the surface with oxygen (10^{-7} mbar/10 min 500 °C) to remove carbon contamination, and then repeatedly sputtered and annealed (Ar^+ 1 kV/6 μA 650 °C). This procedure was continued until sulfur was no longer segre-

gated from the interior of the crystal and a sharp 1×1 low-energy electron-diffraction (LEED) pattern was obtained. Subsequently, the $p(2\times2)$ and $c(2\times2)$ sulfur overlayer structures were obtained by dosing the clean nickel surface, at room temperature, with 1 and 50 L of H_2S, respectively. Following the adsorption procedure the sample was flash annealed to 200 °C to desorb any remaining hydrogen, the surface of the crystal having been cleaned between each adsorption stage. The formation of the overlayer structures were then confirmed by examination of the LEED patterns produced following adsorption.

The clean and sulfated nickel surfaces produced using the procedure outlined above were examined in an Omicron UHV-STM, at a background pressure of the order of 10^{-10} torr, where the different surfaces were imaged using a tungsten tip which had been sputtered prior to use. The three surfaces produced were examined using both topographic and spectroscopic analysis modes. The topographic scans were obtained using the standard constant current mode, whereas the spectroscopic analyses were obtained by holding the tip above the surface at a constant bias voltage and then momentarily breaking the feedback loop and ramping the voltage over the desired energy range. This procedure is designed to maintain the tip at a fixed height above the surface during the spectroscopy. The z scale on the piezoelectric drive was internally calibrated using the steps on the clean nickel surface, where the theoretical nickel step height was taken as 1.76 Å.

III. EXPERIMENTAL RESULTS

Clean nickel

Following the crystal cleaning procedure, described above, the clean nickel (100) surface was imaged. The surface was observed to have a relatively high step density, with the step edges running in the [011] direction. Screw dislocations emerging from the surface were also prevalent. However, broad terraces several hundred Å wide were common, and on these terraces atomic resolution could be obtained (Fig. 1). It was found that the clean surface could be imaged between ±100 mV and 1–2 nA, but that the optimum imaging conditions were found to be -15 mV and 2 nA. These imaging conditions produced a surface corrugation amplitude of 0.12 and 0.08 Å in the [001] and [011] directions, respectively. The magnitude of this corrugation is slightly larger than that reported by Kopatzki and Behm for the same surface,[23] although the difference in the optimum corrugation height observed between the two investigations is probably attributable to the different tunneling currents used, Kopatzki and Behm using a tunneling current of 1 nA. Measurement of the interatomic distances from the STM images gave a primitive lattice parameter of 2.82 Å, which is 13.3% larger than the correct value, as determined by x-ray diffraction. This overestimate of the lattice parameter is primarily attributable to calibration errors in the X-Y piezoelectric scanners, thermal drift and/or piezoelectric creep.

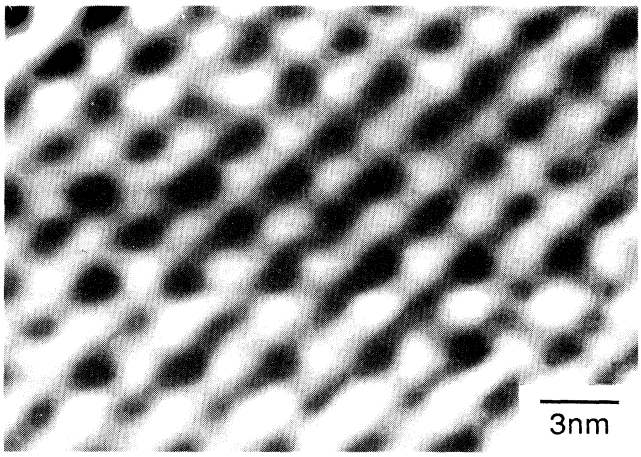

FIG. 1. The atomic resolution image of the clean Ni(100) surface (-15 mV/2 nA).

Nickel–$p(2\times2)$ sulfur

Following the adsorption of 1 L of H_2S onto the clean surface, the STM imaging conditions were observed to have altered drastically compared with the conditions employed on the clean surface. The optimum imaging conditions were obtained at 1 nA and between $+2$ and $+3$ V, conditions more often associated with the imaging of semiconductor surfaces. A significant change in the tunneling conditions has been a common feature in a number of gas-metal adsorption studies.[17] Under these conditions, a well-ordered $p(2\times2)$ sulfur overlayer was formed (Fig. 2), which when imaged at 3 V exhibited a corrugation height, in the [001] direction, of 0.24 Å. On decreasing the voltage to 2 V, the corrugation height was observed to be almost unaltered (see Table I). Reversing the polarity of the tip had little or no influence on the image of the corrugation heights observed. The $p(2\times2)$ overlayer was observed to extend uniformly across the

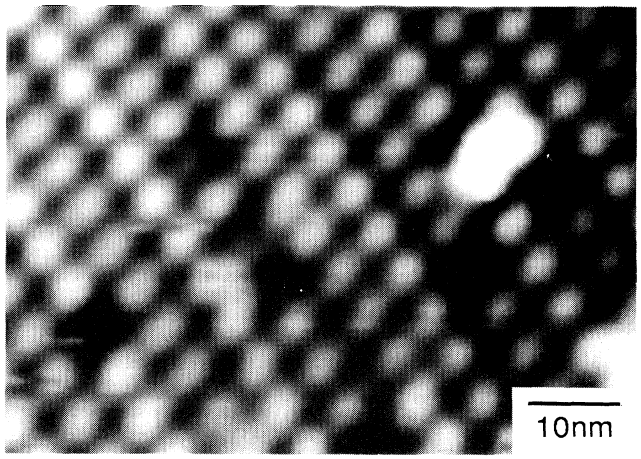

FIG. 2. A well-ordered $p(2\times2)$ sulfur overlayer (3 V/1 nA).

TABLE I. Comparison of experimental and theoretical data for different tunneling conditions.

I (nA)	V_B (V)	Surface	z (Å)	Calculated corrugation (Å)	Experimental corrugation (Å)
2	−0.015	Clean Ni	4.8	0.01	0.10
1	2.0	$p(2\times2)$	6.2	0.25	0.21
1	2.0	$c(2\times2)$	6.7	0.02	Not resolved
1	3.0	$p(2\times2)$	6.6	0.02	0.24
1	3.0	$c(2\times2)$	6.9	0.01	Not resolved

terraces, and appeared to be unaffected by the proximity of either the edge of the terrace or an adjacent step. On the terraces, antiphase domain boundaries (APDB's) were clearly visible, these boundaries having a high density of vacant sites associated with them (Fig. 3). Vacant sites were also observed in the well-ordered areas of the $p(2\times2)$ overlayer, away from the APDB's, and were often observed to form into small clusters. An attempt to image the clean nickel substrate within one of these small sulfur-free areas proved unsuccessful. However, it was observed that the height of the sulfur atoms above the clean nickel surface was only 0.5 Å, which is much smaller than would be expected on the basis of geometrical considerations alone. It is apparent that the S-Ni step height is strongly influenced by electronic effects, as has been observed in many other systems.[17]

From an examination of the structure of the sulfur overlayer in the vicinity of the APDB's, it is evident that the sulfur atoms never occupy nearest-neighbor or next-nearest-neighbor sites [Fig. 3(b)]. This is consistent with the work of McGrath *et al.*,[5,24] which suggests that the nearest-neighbor sites on the Ni(100) surface is strongly repulsive, the second-nearest-neighbor site is weakly repulsive, while the third-nearest-neighbor site is attractive. Furthermore, areas of $c(2\times2)$S were not observed anywhere on the sample, which is consistent with the fact that if the first- and second-nearest-neighbor sites are high-energy sites, the H_2S molecules preferring to diffuse across the $p(2\times2)$S-Ni surface to vacant sites, rather than forming a $c(2\times2)$S overlayer.

Nickel–$c(2\times2)$ sulfur

Following the adsorption of 50 L of H_2S onto the surface, it was expected that the surface would be saturated in sulfur, since previous investigations have indicated that the (100) nickel surface becomes saturated after an exposure of 3–6 L of H_2S.[25] However, on imaging the surface (±2 V/1 nA), it was evident that far from producing saturation, the $c(2\times2)$ sulfur overlayer only accounted for approximately 50–60% of the surface area (Fig. 4), the remainder of the surface being covered in a $p(2\times2)$ overlayer. The strong $c(2\times2)$ LEED pattern obtained from the surface, with only extremely weak $p(2\times2)$ spots present, indicates that the bright regions in the image must have a $c(2\times2)$ structure, even though the $c(2\times2)$ unit cell is not resolved. This observation confirms the earlier work of Perdereau and Oudar,[26] who performed a LEED study of the clean and sulfated low index nickel surfaces; the sulfur surface coverage was determined using the β-emitter S^{35}. They reported that a sharp $c(2\times2)$ LEED pattern was formed on Ni(100) at only 80% saturation. This observation reveals the limitations of LEED patterns in accurately defining the condition of overlayer structures, and has important implications in areas where an accurate knowledge of the surface coverage is required. Recently an investigation of the Au-on-Si system in the STM has shown similar disparities between the observed LEED patterns and the true

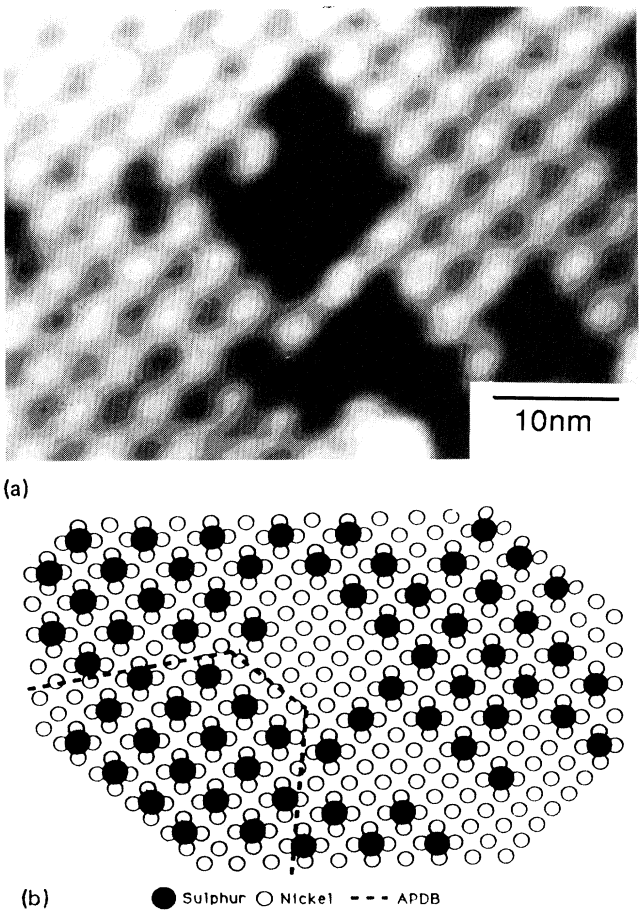

FIG. 3. (a) The antiphase domain boundary (APDB) in the $p(2\times2)$ overlayer, with a high density of vacant sites associated with it (3 V/1 nA). (b) Schematic outlined area in (a), indicating the path of the APDB (dotted line), and showing that the nearest-neighbor and next-nearest-neighbor sites are not occupied in the low-coverage condition.

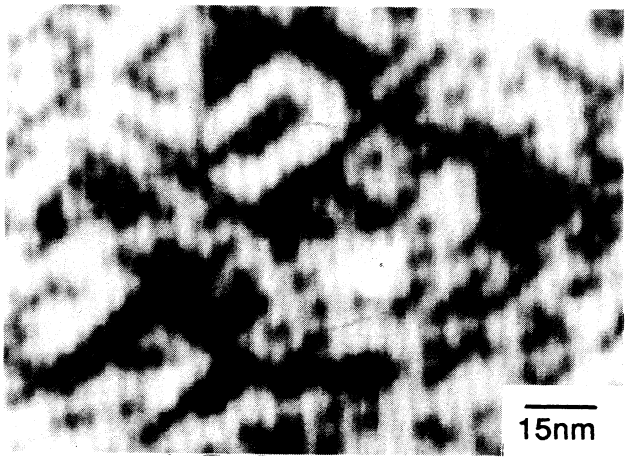

FIG. 4. A $p(2\times2)$-$c(2\times2)$ "mixed overlayer" formed following the adsorption of 50 L of H_2S (2 V/1 nA). The bright regions are unresolved areas of $c(2\times2)$ S.

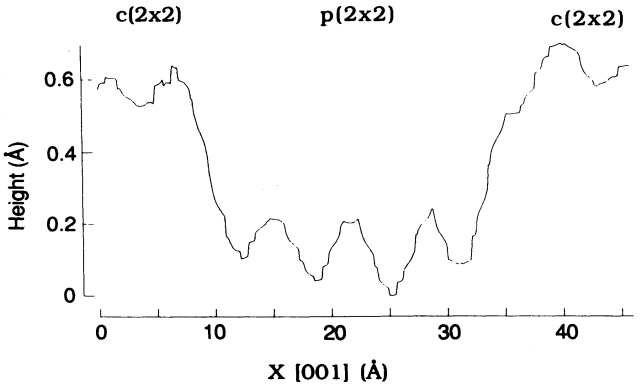

FIG. 5. The topographic line profile of two $c(2\times2)$ regions separated by a small area of $p(2\times2)$. The line profiles show the large difference in height between the two phases.

state of the surface structure.[27] A number of other investigations have also shown that the maximum sulfur coverage obtained during H_2S dosing was only 0.4 monolayer (ML), and that to achieve saturation requires doses greater than 30 L and/or the use of elevated dosing temperatures.[28]

Apart from the fact that the nominally saturated $c(2\times2)$ surface is actually a "mixed" overlayer" structure, the most striking feature of the STM image is the differences between the $p(2\times2)$ and $c(2\times2)$ areas of the sample. First, the bright regions in the image, which have been identified, using LEED, as $c(2\times2)$ regions are not resolved in the image. Although the interatomic distance between the sulfur atoms in the $c(2\times2)$ unit cell is 30% smaller than the $p(2\times2)$ unit cell, it is unlikely that the loss of resolution is attributable to the reduced size of the unit cell, since the clean nickel surface had previously been imaged (although a change in the condition of the tip cannot be ruled out). It would therefore appear that the apparent loss of resolution may be attributable to a significant change in the electronic structure, producing a consequent reduction in the $c(2\times2)$ corrugation height. Second, it is evident that there is a large difference in the relative height of the $p(2\times2)$ and $c(2\times2)$ areas. Height profiles taken from the intersection of the two phases show that the tip withdraws up to 0.6 Å as it crosses from a $p(2\times2)$ area into a $c(2\times2)$ area (Fig. 5). A recent LEED investigation of the $p(2\times2)$ and $c(2\times2)$ sulfur overlayers on nickel, using a computer controlled AUTOLEED system,[3] indicated that the overall relative displacement of the $p(2\times2)$ surface to the $c(2\times2)$ surface, including first- and second-layer nickel substrate relaxation effects, is only of the order of 0.05 Å. Similarly, a recent surface-extended x-ray-absorption fine-structure (SEXAFS) determination of the first-layer relaxation of nickel, induced by the presence of $p(2\times2)$ and $c(2\times2)$ sulfur overlayers, indicates a height difference of only ~0.07 Å.[4] This indicates that the variation in height between the two sulfur phases, observed in the STM, is primarily attributable to a change in the surface electronic structure.

Furthermore, it was observed that the difference in the relative height of the two phases appeared to be effected by the lateral size of the $c(2\times2)$ areas. Isolated $c(2\times2)$ atoms and small clusters of $c(2\times2)$ atoms exhibited a vertical displacement of only 0.3–0.4 Å, with regard to the $p(2\times2)$ phase, whereas large areas of $c(2\times2)$ atoms displayed vertical displacements of up to 0.6 Å. This provides further evidence that the height difference observed between the two phases is predominantly electronic in origin, since any geometric rearrangement caused by an increase in the size of a $c(2\times2)$ overlayer would be extremely small.

Spectroscopy

I-V and *dI/dV* curves were obtained from all three surfaces. In each case, except on the clean nickel, the spectroscopy curves were obtained using a tip which was simultaneously producing atomic resolution images. On the clean nickel surface, although atomic resolution had been lost, terraces and monoatomic steps were still clearly visible.

Spectroscopy curves were obtained from the clean nickel surface at three bias voltages (1, 2, and 3 V; 1 nA), the tip energy being ramped between +3 and −3 V in each case. All the conductivity curves exhibited a fairly featureless parabolic behavior, centered around the Fermi energy.

The subsequent formation of the "mixed overlayer" phase on the nickel surface had the advantage that conductivity curves could be obtained from the $c(2\times2)$ and $p(2\times2)$ surfaces under identical conditions. These curves showed a similar type of behavior to the clean nickel surface, although some weak structure was clearly visible between +2 and −2 V. The two structures generally exhibited a similar behavior over the voltage range studied, although on reducing the bias voltage from 3 to 2 V there was a large increase in the $p(2\times2)$ conductivity at +3 V, which was not evident in the $c(2\times2)$ structure (Fig. 6). These features are discussed further in Sec.

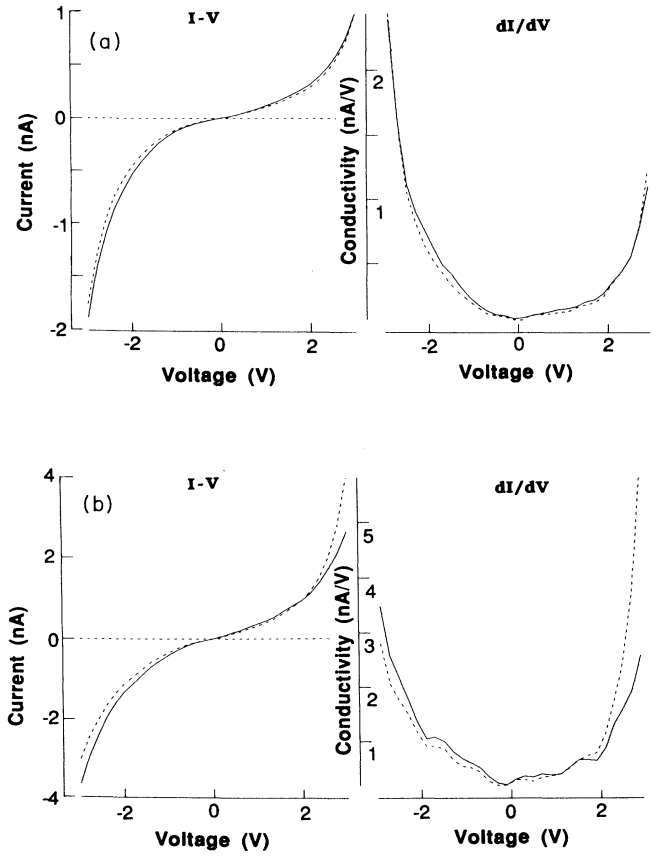

FIG. 6. (a) Experimental conductivity curves for the $p(2\times2)$ (dotted line) and $c(2\times2)$ (full line) surfaces obtained at 3 V/1 nA. (b) Experimental conductivity curves for the $p(2\times2)$ (dotted line) and $c(2\times2)$ (full line) surfaces obtained at 2 V/1 nA, showing the large increase in the $p(2\times2)$ conductivity at +3 V.

V. In addition, since atomic resolution was achieved on the $p(2\times2)$ structure, it was possible to obtain high spatial resolution spectroscopy data from this phase. However, no significant difference in the I-V or conductivity curves could be detected between spectra obtained from different positions on the surface (i.e., between atop sites and fourfold hollow sites).

It should be noted that occasionally spectroscopic data were obtained on the sulfated Ni surfaces which contained apparently spurious structure. The origin of this structure has been attributed to tip changes, possibly occurring as a consequence of adsorption onto the end of the tip. Changes in the tip structure effect the spectroscopy by altering the area of the surface analyzed in an analogous way to that with which they effect the lateral spatial resolution of the images. However, although the adsorption of a foreign atom onto the apex of the tip may have little effect on the lateral resolution of the images, it can have a very significant effect on the spectroscopy, particularly when the adsorbate atom strongly modifies the tip's electronic structure. These problems have to be borne in mind when analyzing STM spectroscopy data.

IV. THEORY

Our description of the STM is based on the theory of Pendry, Pretre, and Krutzen.[2] It is a Green's-function-based method which in its general formulation takes the mutual perturbation of tip and sample into account. However, by replacing the total Green's function in the center of the tunneling barrier by the free Green's function (G_0), one can deduce Bardeen's approximation, where the electron states of the unperturbed tip and sample are considered. This procedure has been used in the present work. The tunneling conductivity is then given by

$$\frac{dj_T}{dV}=\frac{2e^2}{\hbar\pi}\left[\frac{\hbar^2}{2m}\right]^2 \mathrm{tr}[(\overleftarrow{\nabla}-\vec{\nabla})\Im G_{\mathrm{tip}}(\overleftarrow{\nabla}-\vec{\nabla})\Im G_{\mathrm{sample}}]\ . \tag{1}$$

The trace implies integration over an interface between tip and sample. The sample Green's function is calculated in a multiple-scattering formalism based on the layer KKR method.[22] The atoms are described as spherically symmetric scattering centers, and the surface barrier is approximated by a step potential. The Green's function of the tip is expanded in a basis of spherical functions centered on the foremost tip atom. The electronic structure of the tip is then described by a site-diagonal scattering path operator.[29] This quantity can be found using, for example, a cluster calculation.[30,31] However, since the geometric structure of the tip is unknown, and subject to changes, we describe it by a single atom. Thus the scattered part of the tip Green's function at negative energies (referred to the vacuum zero) can be written as

$$\begin{aligned}G^s_{\mathrm{tip}}(\mathbf{r},\mathbf{r}',E)&=G_{\mathrm{tip}}(\mathbf{r},\mathbf{r}',E)-G_0(\mathbf{r},\mathbf{r}',E)\\&=(2\kappa_0)^2\sum_{lm,l'm'}(-i)^{l+l'}k_l(\kappa_0 r)\\&\quad\times Y_{lm}(\hat{r})t_{lm,l'm'}(E)\\&\quad\times k_{l'}(\kappa_0 r')Y^*_{l'm'}(\hat{r}')\ ,\end{aligned} \tag{2}$$

where $\kappa_0=\sqrt{-2E}$ in atomic Hartree units. $t_{lm,l'm'}(E)$ is the T matrix of the tip atom and k_l is a modified spherical Bessel function. Only the scattered part is needed for the tunneling problem, since the free Green's function is real at negative energies and it is the imaginary part that enters the tunneling expression (1). A single atom is a finite system and cannot take up current, and its electronic structure at negative energies consists of discrete bound states. Therefore, to introduce the effects of an extended system, we take the T matrix of the tip atom at a complex energy. This makes the scattering absorptive, allowing current to flow into the tip, and causes the bound states to broaden, thereby enabling tunneling processes to occur over a continuous energy range. The imaginary part of the energy should be of the order of the bandwidth of the tip.

Restricting the expansion of the tip Green's function to $l=0$, we recover the s-wave approximation of Tersoff and Hamann,[32] which at zero bias makes the STM conductivity proportional to the local density of states.

At vanishing bias voltage V_B, Eq. (1) is equal to the conductivity. However, on the application of a finite voltage, it is necessary to integrate the expression over the allowed energy range to obtain the total tunnel current, taking into account that the Fermi energies of the tip and sample differ by V_B. Expanding G_{tip} and G_{sample} into suitable basis sets, the STM current $I(V_B)$ is given by a sum over terms (i), each of which is of the form

$$i = \int_0^{V_B} dE\, f_T(E - V_B) f_S(E) , \tag{3}$$

where f_T and f_S are tip- and sample-related functions. Here $E = 0$ refers to the Fermi energy.

The conductivity dI/dV_B can thus be determined such that

$$\frac{dI}{dV_B} = f_T(0) f_S(V_B) - \int_0^{V_B} dE \left[\frac{df_T(E - V_B)}{dE} \right] f_S(E) . \tag{4}$$

The equation is composed of two terms, the first originating from the upper integral boundary (a counting term which arises from the fact that more states are tunneling at increasing v_B), and the second which takes into account the relative shift of the two energy scales.

Thus the conductivity contains an integral over energy just as the current does, and the numerical computation is consequently made no easier. However, by taking advantage of the fact that wave functions with the highest energy dominate the tunneling current since the exponential tails of the high-energy wave functions protrude further into the vacuum barrier, the second term in Eq. (4) can, to a first approximation, be discarded. This approximation facilitates the numerical calculation considerably and allows us to evaluate the conductivity using states at a single energy only. Having thus obtained the conductivity, the current is then calculated by numerical integration. Comparing the integrand $f_T(0) f_S(E)$ of that integration with Eq. (3), we see that the approximation simply consists of taking the tip function at its highest energy, instead of its actual energy. In the argument given above, it was assumed that the sample was positively biased, so that the tip is the system higher in energy. For negative bias, the roles of f_T and f_S are simply reversed.

The use of the single-energy approximation introduces several possible sources of error which need to be considered. First, the error introduced by this single-energy approximation increases as E-V_B differ from zero (i.e., in general for larger voltages). In the context of our calculations this means that the results for 2 V/1 nA are more reliable than those for 3 V/1 nA. Second, as can be seen from Eq. (4), sharp peaks in the tip function f_T (through the presence of surface states, for instance) will make the omission of the integral questionable. Fortunately, our model tip has a fairly smooth electronic structure throughout its occupied energy range, such that this approximation will be good for positive voltages. However, the tip has a sharp s resonance in its unoccupied range, which leads to a peak in the calculated spectrum not observed experimentally (as discussed below). Finally, the approximation is expected to be poor if the character of the tip states vary strongly as a function of energy (i.e., s states dominating at different voltages from that of p states). However, in the present calculation, the tip is described as a single scatterer and it turns out that the s states always dominate when the tunneling current is determined outside the scatterer, at distances greater than approximately 1 Å, and at negative energies.

Independent of this approximation, there is a general tendency in STM spectroscopy to be more sensitive to that component, tip or sample, into which the electrons tunnel. Again this derives from the fact that states highest in energy tend to dominate the tunneling current. If we consider the tip-sample system to be positively biased, such that tip states tunnel into the sample, then, on increasing the voltage by δV_B, the highest state on the tip side of the junction remains approximately unaltered (apart from changes in the barrier shape) while the highest available state on the sample side is now a state δV_B above the previous one. We would therefore expect that the contrast in the $I(V_B)$ spectrum to derive largely from the electronic structure of the sample. At negative bias voltages, on the other hand, the spectrum is more likely to reflect the unoccupied states of the tip. For this reason, we concentrate on positive voltages in the following, because our model of the sample is more elaborate than that of the tip.

To describe the nickel substrate, we have used the non-spin-polarized potential of Moruzzi, Janak, and Williams,[33] while the sulfur muffin-tin potential is constructed from atomic charge densities using the Hartree-Fock-Slater method. The MUFPOT program, available at Daresbury Laboratory, was used for this. The Slater parameter α was chosen so as to obtain the p resonance at 4 eV below the Fermi energy, as indicated by photoemission experiments. This gives $\alpha = \frac{2}{3}$. The space between the adsorbed sulfur atoms is filled with empty spheres, which were located at the unoccupied fourfold hollow sites. The parameters of the spheres were obtained by the requirement that a complete overlayer of them should mimic a slice of vacuum. More specifically, we considered the local density of states (LDOS) at the Fermi level of a clean Ni(100) surface at a given vertical distance. Putting a monolayer of vacuum spheres onto the surface should leave the LDOS unchanged. Taking the constant potential within the spheres to be at the vacuum level, the required radius is 2.46 bohr radii, which is slightly larger than the nickel spheres. The electronic structure of the clean nickel substrate was calculated assuming an unrelaxed first-layer spacing. Although the exact value of the first-layer relaxation reported in the literature varies, it is only of the order of 1%.[34] The geometry of the $p(2\times2)$ and $c(2\times2)$ sulfur overlayers used in the calculations was obtained from various sources.[34]

The work function of the clean nickel (100) surface is taken to be 5 eV,[35] while, for the sulfur-covered surfaces Hardegree, Ho, and White[28] report an increase of the work function of 0.29 and 0.4 eV for coverages of 25% and 50%, respectively. We therefore take the work function to be 5.29 eV for the $p(2\times2)$ structure and 5.4 eV

for the $c(2\times2)$ structure. Similar changes in the work function with increasing sulfur coverage were reported by Anderson.[36] Even if the coverage-induced work-function changes are ignored, our calculations lead to essentially the same conclusions. This is because the work functions of the $c(2\times2)$ and $p(2\times2)$ overlayers are very similar, which makes a comparison between the two cases relatively insensitive to a small change in the absolute value of the work function.

A nickel potential from the bulk was taken to represent the tip atom. In order to produce a reasonable value of the bandwidth of the tip [given approximately by 2 Im(E) in our model], the imaginary part of the energy inside the tip was taken to be 2 eV. The plane of integration for the calculation was fixed at 4 a.u. from the tip center, and the tip Green's function was considered up to $l_{\max}=3$.

V. THEORETICAL RESULTS

Topography

The theory of a STM image of a periodic surface can best be discussed in terms of reciprocal space. The current can be written as a two-dimensional lattice Fourier transform whose coefficients are functions of the tip-sample separation z. The zero-order Fourier coefficient represents the lateral average of the current, and its magnitude as a function of z determines the tip-sample distance. The other Fourier coefficients, corresponding to reciprocal-lattice vectors $\mathbf{G}$, give rise to the observed corrugation, their magnitude rapidly diminishing with increasing $|\mathbf{G}|$. General arguments show that the zero-order coefficient, and thus the tip-sample distance, is influenced mainly by sample states with a parallel momentum $\mathbf{k}_{\parallel}$ around the $\bar{\Gamma}$ point. For the lowest nonzero $\mathbf{G}$, however, and thus for the corrugation, the Brillouin-zone (BZ) boundary is the most important region (see, e.g., Tersoff[37]). We will now present the results of the calculations described in Sec. IV, and discuss them in terms of these simple ideas.

The surface electronic structure of clean Ni(100), at and above E_F, shows a continuum of bulk states around the $\bar{\Gamma}$ point and band gaps at the BZ boundary. Thus at positive bias voltage, i.e., electrons tunneling into the sample, we expect the tip-sample distance to be large, and the surface corrugation to be small, which of course it turns out to be. In order to achieve atomic resolution, a very small bias voltage is required which causes the tip to come into close proximity to the surface. In order to attain the experimental current of 2 nA at -15 mV, our model tip has to come as close as 4.8 Å to the surface (measured between atom centers), which is 1.4–2.1 Å closer than in the adsorbate systems discussed below. Under these circumstances Bardeen's approximation may be inadequate to describe the tunneling junction, and tip-sample interactions may become dominant. Therefore it is not surprising that the calculated corrugation of 0.01 Å is much smaller than the experimentally obtained result of 0.1 Å. However, it is worth noting that magnetic surface states have been identified immediately below E_F,[38] in the energy region where the optimum imaging conditions are observed. These states reside near the BZ boundary, which makes them a possible cause of enhanced corrugation, even in the absence of tip-sample interactions. Our non-spin-polarized calculation shows a similar surface state along $\bar{\Gamma}\bar{X}$, but with a stronger dispersion and residing 0.2 eV below the Fermi level. If we artificially shift the band structure up by 0.2 eV, so that this surface state is included in our calculation, the corrugation is almost doubled; although this is still significantly smaller than the values of 0.05 Å observed by Kopatzki and Behm[23] or 0.1 Å observed in this work. It does suggest, however, that Bardeen's approximation may not completely break down at this distance, and that part of the discrepancy observed between the theory and experiment is attributable to our simple model potential, which is unable to generate the subtleties of the magnetic surface band structure on Ni(100).

On adding a quarter of a monolayer of S to the Ni(100) surface to form the $p(2\times2)$ structure, the BZ boundary is folded back to the $\bar{\Gamma}$ point. We now find a band gap at $\bar{\Gamma}$ above $+1$ eV, and a continuum of states at the boundary. This is the opposite situation to that found on the clean Ni(100) surface. Consequently, if identical tunneling conditions are employed on the two surfaces, the tip has to move closer to the $p(2\times2)$ surface because the previously dominant states at $\bar{\Gamma}$ are missing. For that reason, and because most states reside near the BZ boundary, we obtain a large corrugation of 0.25 Å at $+2$ V/1 nA, which is in good agreement with the observed value. On increasing the bias voltage to 3 V, the calculated $p(2\times2)$ corrugation remains larger than on the $c(2\times2)$ surface, although it is not as large as was observed experimentally (see Table I). However, as mentioned in Sec. IV, we expect the results to become worse at larger voltages because of the single energy approximation, and also because the assumption of a simple step potential at the surface becomes more and more inadequate at higher voltages.

Because the tip is closer to the surface than on the clean Ni, the experimentally observed step height between Ni(100) and $p(2\times2)$ is only 0.5 Å, as opposed to the atomic step height of 1.3 Å determined by LEED.[34] The calculation reproduces this reduction in the step height but overestimates its magnitude. Assuming an unrelaxed Ni top layer, the model predicts a negative step height of -0.01 Å.

On adding a further quarter of a monolayer of S to the Ni surface, we obtain the $c(2\times2)$ structure whose electronic properties are somewhat intermediate between those of Ni(100) and the $p(2\times2)$ overlayer. There is a band gap at the BZ boundary at $\bar{M}$ but not at $\bar{X}$, and there is a gap at $\bar{\Gamma}$ at higher energies (above $+2.5$ eV). Also, immediately above E_F (~0.2 eV) there is a surface state or resonance around the $\bar{\Gamma}$ point. The states at $\bar{\Gamma}$ allow the tip to stay further away from the sample than in the $p(2\times2)$ case. At 2 V/1 nA, the calculated height difference between the $p(2\times2)$ and $c(2\times2)$ surfaces is 0.5 Å. This compares quite well with the experimentally observed height difference of 0.6 Å (see Fig. 7, which should be compared to the experimental data in Fig. 5). It confirms that the height difference observed between

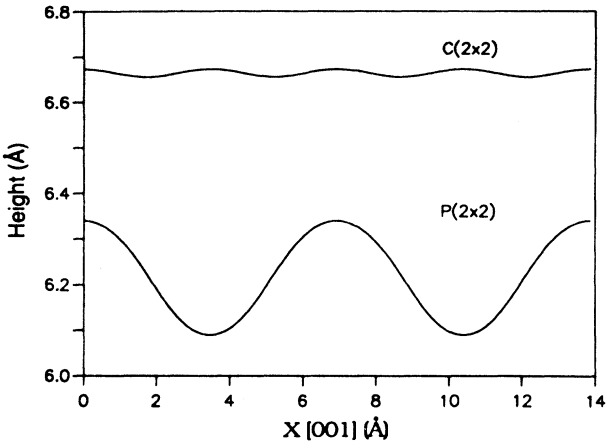

FIG. 7. Calculated corrugation curves for the $p(2\times2)$ and $c(2\times2)$ overlayers, taken in the [001] direction (2 V/1 nA).

the two surfaces is essentially electronic in origin. The $c(2\times2)$ surface is smoother than the $p(2\times2)$ surface because of the larger tip-sample distance and the gap at the BZ boundary, although it is not as smooth as the Ni(100) surface. The calculated corrugation of 0.02 Å at 2 V/1 nA explains why no corrugation was observed on the $c(2\times2)$ areas, since such a small value would not be discernable with the noise level present in the images.

Spectroscopy

The experimental spectra in Fig. 6 were obtained by holding the tip a certain distance from the sample, defined by a voltage V_0 and current I_0. The spectra were then collected by holding the tip in that position while ramping the voltage. Therefore the tip-sample distance varies from one surface to another, due to variations in the surface electronic structures. Figure 6(b) seems to suggest that in going from $V_0=3$ V to $V_0=2$ V, i.e., bringing the tip closer to the sample, a strong effect occurs on the $p(2\times2)$ surface above 2 V which does not occur on the $c(2\times2)$ surface. This might indicate strong tip-sample interactions which would throw doubt on the use of Bardeen's approximation. This behavior is, however, a consequence of the method just described to obtain the spectra. It occurs due to the fact that the current as a function of voltage is pinned at two points, the origin and the point V_0/I_0 used for defining the tip-surface distance (e.g., 2 V/1 nA). Spectra from different types of surfaces, taken with the same V_0/I_0 will all be pinned at the same two points and will therefore tend to look similar between these points, apart from differences in fine structure. If two spectral curves are different, the pinning suppresses their difference between these two points but tends to enhance it outside of the pinned region. Thus in Fig. 6(a), the two curves for the $p(2\times2)$ and $c(2\times2)$ surfaces look very similar because the pinning interval extends from the origin to the highest voltage used (3 V). In Fig. 6(b), however, the curves are pinned at 0 and 2 V/1 nA, and we see that above this interval, there is a marked difference between the curves. On closer inspection, both surfaces exhibit the same trends: the conductivity increases with voltage for both $p(2\times2)$ and $c(2\times2)$, but the increase for $p(2\times2)$ is more pronounced. This trend is reproduced by the calculation, as shown in Fig. 8. It can be explained in terms of the electronic structures. On the $p(2\times2)$ surface, the tip has to stay fairly close the sample because states which would most easily tunnel, near the $\bar{\Gamma}$ point, are not available due to the band gap. As the voltage increases, states at higher energy are picked up which reach out further into the vacuum, causing the current to rise. On the $c(2\times2)$ surface, on the other hand, the tip resides further away from the surface because states at the $\bar{\Gamma}$ point are readily available. With increasing voltage, the gap at the $\bar{\Gamma}$ point opens up so the current does not grow as strongly as it would have done otherwise. Thus we end up with $p(2\times2)$ curve increasing more rapidly than $c(2\times2)$ curve. The rise in the theoretical conductivity of the $c(2\times2)$ curve at 1 V is due to the presence of the surface state above E_F, as mentioned previously. It is tempting to associate this rise with the similar structure apparent in the corresponding experimental curve in Fig. 6(b), but this may be coincidental because other structures at

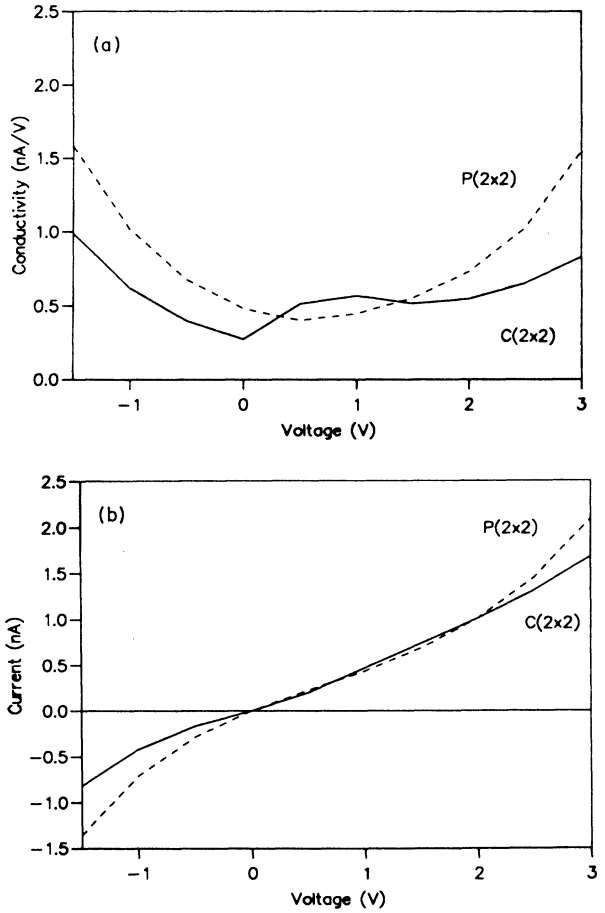

FIG. 8. (a) Calculated conductivity curves for the $p(2\times2)$ and $c(2\times2)$ overlayers (2 V/1 nA). (b) Calculated tunneling currents for the $p(2\times2)$ and $c(2\times2)$ overlayers (2 V/1 nA).

higher voltages are not reproduced. Generally, we would not expect our non-self-consistent muffin-tin model potential to generate all the small-scale structure visible in Fig. 6(b) (although in a recent self-consistent full-potential calculation,[39] a surface state was found at this energy as well). However, the energy mesh size in this calculation was 0.5 eV, so we cannot expect to explain details of the spectra with a smaller size than this. What we are attempting to produce in the calculation is general trends which have been well reproduced.

At negative voltages the calculation produces a larger current than that produced at positive voltages. This reflects the fact that the $p(2\times2)$ and $c(2\times2)$ surfaces have occupied states at the Fermi energy around the $\bar{\Gamma}$ point, and that the electronic structure of the tip does not contain a band gap, so that we would expect a larger current at negative voltages. The experimental spectra in Fig. 6 also show this asymmetry, with the exception of the $p(2\times2)$ curve at 2 V/1 nA [Fig. 6(b)], the behavior of which we cannot account for. There is also a peak in the theoretical conductivity at -2.5 V (not shown in Fig. 8) which is an artifact of the theory. It is attributable to the s-state resonance used to describe our single-atom tip (see Sec. IV). In order to obtain an improved spectrum at negative voltages, we would need to define a better tip model, such as a cluster model. Finally, the fact that the $p(2\times2)$ conductivity is larger than the $c(2\times2)$ conductivity at negative bias, which is at variance with the experimental results, may partly be a consequence of the single energy approximation described in Sec. IV. However, we should also take into account the fact that the tip distance z in the calculation was adjusted to obtain a certain current I_0 at a positive bias V_0. Since our model contains several approximations, the value of z will not be exact, and the current is very sensitive to changes in z. Assuming a behavior of the form $\exp(-2\kappa z)$, where $\kappa=\sqrt{-2E}$ in atomic units, a change in distance $\delta z = 0.1$ Å causes the current to change by about 20%. Thus errors in the calculation of z are likely to play a role in the differences observed between the theoretical and empirical spectroscopy curves at negative voltages.

In conclusion, our simple model has proved quite successful. The calculated corrugation heights on the sulfated nickel surfaces are consistent with those observed in the images obtained at 2 V, while the height difference observed between the $p(2\times2)$ and $c(2\times2)$ overlayers is reproduced. In addition, the model has confirmed the fact that the height difference between the two phases is predominantly electronic in origin. This is consistent with the observed dependence of the height difference on the lateral size of the $c(2\times2)$ overlayer. The calculated corrugation of the clean nickel surface was significantly smaller than was observed experimentally. However, the approximate inclusion of the magnetic surface state located immediately below the Fermi level produces some increase in the corrugation, which suggests that the simplicity of our model potential is partly to blame.

The model also accounts for the overall trends in the spectroscopy, at least for positive voltages and on a scale greater than 0.5 eV. However, smaller structure observed in the experimental spectra could not be accounted for, and at negative voltages the use of a single-atom tip was observed to generate an artificial peak in the conductivity.

Finally, it should be stressed that our model potential is not inherent to the theoretical method. What enters the tunneling expression (1) are the Green's functions of the sample and the tip, so any method of obtaining these Green's functions can be used as a starting point to generate STM data from them. Work is in progress along these lines, involving the method of surface-embedded Green's functions developed by Ingelsfield and coworkers.[39–41] Similarly, there is no conceptual difficulty in improving the tip by using cluster techniques which are readily available.

VI. CONCLUSIONS

Experimental data have been presented for the clean $p(2\times2)$ and $c(2\times2)$ sulfated Ni(100) surface. Changes in the corrugation heights with adsorption and variations in the tip-sample distance with sulfur coverage were observed. Compared to extensive investigations already carried out on this system, the observations suggest that the STM images are dominated by the surface electronic structure rather than by changes in the surface geometry. This analysis was subsequently confirmed by modeling the STM tip-sample system using the Green's-function method of Pendry, Pretre, and Krutzen.[21] This simple model has proved remarkably successful in predicting the corrugation heights of the two sulfated surfaces considered, and confirmed the fact that the difference in height observed between the $p(2\times2)$ and $c(2\times2)$ phases is electronic in origin. Furthermore, it is proposed that the magnitude of the corrugation measured on the clean nickel surface may in part be attributable to the presence of a magnetic surface state immediately below E_F. All the details in the spectroscopic data could not be accounted for, but the main trends at positive voltage were reproduced and could be explained in terms of the surface electronic structures.

ACKNOWLEDGMENTS

We would like to extend our thanks to J. E. Inglesfield, S. Crampin, and J. B. A. N. van Hoof for many useful discussions, and for allowing us access to unpublished data obtained using their surface-embedded Green's-function calculations, and to A. W. Robinson for technical assistance during the course of the experiment. G.H. would also like to acknowledge the financial support of British Petroleum plc.

*Present address: Faculty of Physics, Eindhoven University of Technology, P.O. Box 513, 5600 MB Eindhoven, The Netherlands.

[1]J. Oudar, in *Metal-Support and Metal-Additive Effects in Catalysis, Studies in Surface Science and Catalysis,* edited by B. Imelik, C. Naccache, G. Coudurier, H. Prauliaud, P. Meriaudeau, P. Gallezot, G. A. Martin, and J. C. Vedrine (Elsevier, Amsterdam, 1982), Vol. 11, p. 255.

[2]J. M. MacLaren, J. B. Pendry, D. D. Vvedensky, and R. W. Joyner, Surf. Sci. **162**, 322 (1985).

[3]U. Starke, F. Bothe, W. Oed, and K. Heinz, Surf. Sci. **232**, 56 (1990); W. Oed, U. Starke, F. Bothe, and K. Heinz, Surf. Sci. **234**, 72 (1990); W. Oed, U. Starke, K. Heinz and K. Muller, J. Phys. Condens. Matter **3**, S223 (1992).

[4]F. Sette, T. Hashizume, F. Comin, A. A. MacDowell, and P. H. Citrin, Phys. Rev. Lett. **61**, 1384 (1988).

[5]R. McGrath, A. A. MacDowell, T. Hashizume, F. Sette, and P. H. Citrin, Phys. Rev. B **40**, 9457 (1989).

[6]D. R. Warburton, P. L. Wincott, G. Thornton, F. Quinn, and D. Norman, Surf. Sci. **211/212**, 79 (1989).

[7]D. R. Warburton, G. Thornton, D. Norman, C. H. Richardson, R. McGrath, and F. Sette, Surf. Sci. **189/190**, 495 (1987).

[8]D. H. Rosenblatt, S. D. Kevan, J. G. Tobin, R. F. Davis, M. G. Mason, D. R. Denley, D. A. Shirley, Y. Huang, and S. Y. Tong, Phys. Rev. B **26**, 1812 (1982).

[9]Th. Fauster, H. Durr, and D. Hartwig, Surf. Sci. **178**, 657 (1986).

[10]J. J. Barton, C. C. Bahr, S. W. Robey, Z. Hussain, E. Umbach, and D. A. Shirley, Phys. Rev. B **34**, 3807 (1986).

[11]G. B. Fisher, Surf. Sci. **62**, 31 (1977).

[12]T. T. Anh Nguyen and R. C. Cinti, Surf. Sci. **68**, 566 (1977).

[13]E. W. Plummer, B. Tonner, N. Holzwarth, and A. Liebsch, Phys. Rev. B **21**, 4306 (1980).

[14]L. E. Klebanoff, R. K. Jones, D. T. Pierce, and R. J. Celotta, Phys. Rev. B **36**, 7849 (1987).

[15]H. D. Hagstrum and G. E. Becker, Phys. Rev. Lett. **22**, 1054 (1969); H. D. Hagstrum and G. E. Becker, J. Chem. Phys. **54**, 1015 (1971).

[16]Pei-Lin Cao, D. E. Ellis, and A. J. Freeman, Phys. Rev. B **25**, 2124 (1982).

[17]R. J. Behm, in *Scanning Tunneling Microscopy and Related Techniques,* edited by R. J. Behm, N. Garcia, and H. Rohrer, Volume 184 of *NATO Advanced Study Institute, Series E* (Kluwer, Amsterdam, 1990), p. 173.

[18]S. Rousset, S. Gauthier, O. Siboulet, W. Sacks, M. Belin, and J. Klein, J. Vac. Sci. Technol. **A8**, 302 (1990).

[19]B. Marchon, D. F. Ogletree, M. E. Bussell, G. A. Somorjai, M. Salmeron, and W. Siekhaus, J. Microsc. **152**, 427 (1988).

[20]D. F. Ogletree, R. Q. Hwang, D. M. Zeglinski, A. Lopez Vazquez-de-Parga, G. A. Somorjai, and M. Salmeron, J. Vac. Sci. Technol. B **9**, 886 (1991).

[21]J. B. Pendry, A. B. Pretre, and B. C. H. Krutzen, J. Phys. Condes. Matter **3**, 4313 (1991).

[22]J. M. MacLaren, S. Crampin, D. D. Vvedenski, and J. B. Pendry, Phys. Rev. B **40**, 12 164 (1989).

[23]E. Kopatzki and R. J. Behm, Surf. Sci. **245**, 255 (1991).

[24]R. McGrath, A. A. McDowell, T. Hashizume, F. Sette, and P. H. Citrin, Phys. Rev. Lett. **64**, 575 (1990).

[25]A. G. Baca, M. A. Shultz, and D. A. Shirley, J. Chem. Phys. **81**, 6304 (1984).

[26]J. Perdereau and J. Oudar, Surf. Sci. **20**, 80 (1970).

[27]C. F. J. Flipse (1992) (private communication).

[28]E. L. Hardegree, Pin Ho, and J. M. White, Surf. Sci. **165**, 488 (1986).

[29]J. S. Faulkner and G. M. Stocks, Phys. Rev. B **21**, 3222 (1980).

[30]R. W. Joyner, J. B. Pendry, D. K. Saldin, and S. R. Tennison, Surf. Sci. **138**, 84 (1984).

[31]J. M. MacLaren, J. B. Pendry, D. D. Vvedenski, and R. W. Joyner, Surf. Sci. **162**, 322 (1985).

[32]J. Tersoff and D. R. Hamann, Phys. Rev. B **31**, 805 (1985).

[33]V. L. Moruzzi, J. F. Janak, and A. R. Williams, *Calculated Electronic Properties of Metals* (Pergamon, New York, 1978).

[34]Measurements of the first layer relaxation of clean nickel have been made by J. E. Demuth and D. W. Jepsen, Phys. Rev. B **11**, 1460 (1975); J. W. M. Frenklen *et al.*, Phys. Rev. Lett. **51**, 1876 (1983); X. Oed *et al.*, Surf. Sci. **224**, 179 (1989). The geometry of the $p(2\times2)$ and $c(2\times2)$ overlayers was taken from M. A. van Hove and S. Y. Tong, J. Vac. Sci. Technol. **12**, 230 (1975); J. MacLaren *et al.*, *Surface Crystallographic Information Service* (Reidel, Dordrecht, 1987), respectively.

[35]*The Handbook of Chemistry and Physics,* 51st ed. (The Chemical Rubber Company, Cleveland, Ohio, 1970), gives values of the clean nickel work function ranging from 4.32 to 5.1 eV; however, a recent calculation of bremsstrahlung isochromat spectra (BIS) by G. Thorner and G. Borstel, Solid State Commun. **49**, 479 (1984), obtained good agreement with experiment by assuming a work function of 5.07 eV.

[36]S. Anderson, Surf. Sci. **79**, 385 (1979).

[37]J. Tersoff, Phys. Rev. B **39**, 1052 (1989).

[38]E. W. Plummer and W. Eberhardt, Phys. Rev. B **20**, 1444 (1979).

[39]J. B. A. N. van Hoof, S. Crampin, and J. E. Inglesfield (private communication), (unpublished).

[40]J. E. Inglesfield and G. A. Benesh, Phys. Rev. B **37**, 6682 (1988).

[41]S. Crampin, J. B. A. N. van Hoof, M. Nekovee, and J. E. Inglesfield, J. Phys. Condens. Matter **4**, 1475 (1992).

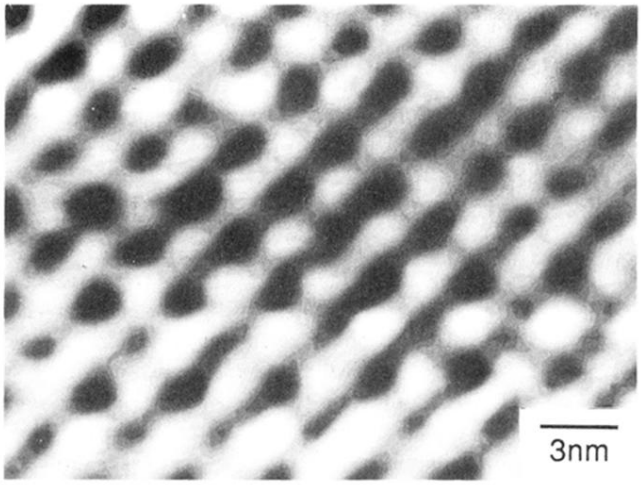

FIG. 1. The atomic resolution image of the clean Ni(100) surface (−15 mV/2 nA).

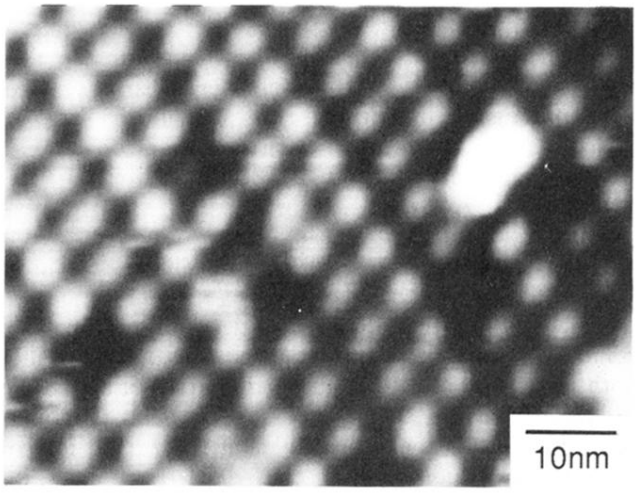

FIG. 2. A well-ordered $p(2\times2)$ sulfur overlayer (3 V/1 nA).

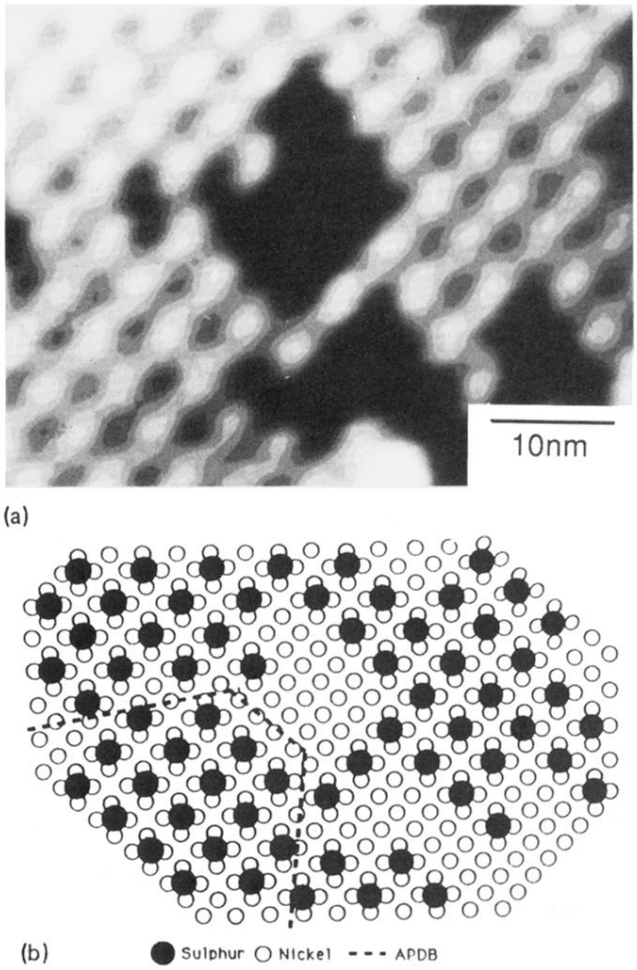

FIG. 3. (a) The antiphase domain boundary (APDB) in the $p(2\times2)$ overlayer, with a high density of vacant sites associated with it (3 V/1 nA). (b) Schematic outlined area in (a), indicating the path of the APDB (dotted line), and showing that the nearest-neighbor and next-nearest-neighbor sites are not occupied in the low-coverage condition.

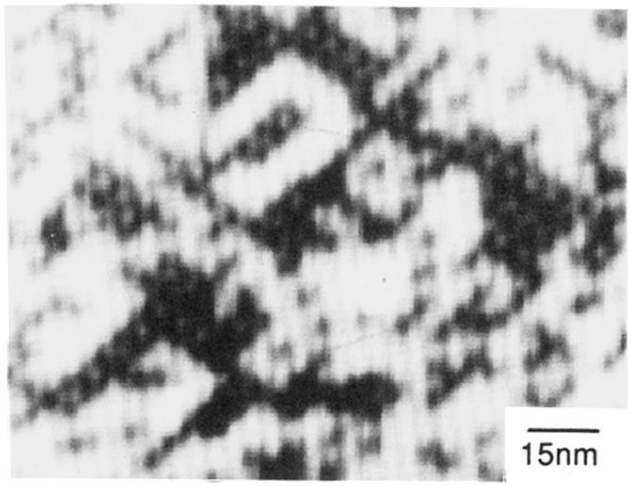

FIG. 4. A $p(2\times2)$-$c(2\times2)$ "mixed overlayer" formed following the adsorption of 50 L of H_2S (2 V/1 nA). The bright regions are unresolved areas of $c(2\times2)$ S.